Vanillin: An Effective Additive to Improve the Longevity of Zn Metal Anode in a 30 *m* $ZnCl_2$ Electrolyte

David Hoang[1], Yaqiong Li[2], Min Soo Jung[1,3], Sean K. Sandstrom[1], Alexis M. Scida[1], Heng Jiang[1], Trenton C. Gallagher[1], Brenden A. Pollard[1], Rachel Jensen[1], Nan-Chieh Chiu[1], Kyriakos Stylianou[1], William F. Stickle[4], P. Alex Greaney*[2], and Xiulei Ji*[1]

[1]Department of Chemistry, Oregon State University, Corvallis, Oregon, 97331, United States
[2]Department of Materials Science and Engineering, University of California, Riverside, California, 92521, United States
[3]School of Chemical and Biological Engineering, Seoul National University; Seoul, 08826, Republic of Korea
[4]Hewlett-Packard Co., 1000 NE Circle Blvd., Corvallis, Oregon, 97330, United States

*E-mail: david.ji@oregonstate.edu, agreaney@engr.ucr.edu

Keywords: Vanillin, SEI, $ZnCl_2$, Zn metal anode, Coulombic efficiency

Abstract: It remains a challenge to design aqueous electrolytes to secure the complete reversibility of zinc metal anode. The concentrated water-in-salt electrolytes, *e.g.*, 30 *m* $ZnCl_2$, are promising candidates to address the challenges of the Zn metal anode. However, the pure 30 *m* $ZnCl_2$ electrolyte fails to deliver a smooth surface morphology and a practically relevant Coulombic efficiency. Herein, we report that a small concentration of vanillin, 5 mg/mL_{water}, added to 30 *m* $ZnCl_2$ transforms the reversibility of Zn metal anode by eliminating dendrites, lowering the Hammett acidity, and forming an effective solid electrolyte interphase. The presence of vanillin in the electrolyte enables the Zn metal anode to exhibit a high Coulombic efficiency of 99.34% at a low current density of 0.2 mA/cm^2, at which the impacts of the hydrogen evolution reaction are allowed to play out. Using this new electrolyte, a full cell Zn metal battery with an anode/cathode capacity (N/P) ratio of 2:1 demonstrates no capacity fading over 800 cycles.

1. Introduction

Aqueous zinc metal batteries (ZMBs) have garnered much attention for grid storage applications due to the innate safety advantages and the attributes of Zn metal anode (ZMA), including high theoretical capacity, *i.e.*, 820 mAh/g,[1] low operating potential, *i.e.*, –0.76 V vs. standard hydrogen electrode (SHE), and natural abundance.[2] The market values of storage batteries are evaluated by the levelized energy cost (LEC), which is the expense of the electricity to be delivered from the storage facility over its lifetime. However, the low capital cost of aqueous metal batteries cannot be translated to a competitive LEC unless the cycle life of such batteries is comparable with that of Li-ion batteries, *e.g.*, thousands of deep cycles. This has been a long-standing challenge of aqueous metal batteries. For example, the LEC of lead-acid batteries is not competitive compared to Li-ion batteries due to their short cycle life.[3]

For ZMBs, the failure to deliver the promised energy density and long cycle life is primarily due to the poor reversibility of the Zn plating and stripping processes of ZMA in a battery's charge and discharge, respectively. The extent of the reversibility of ZMA is measured by the Coulombic efficiency (CE), and over the past decade, tremendous effort has been devoted to improving the CE of ZMA in mildly acidic electrolytes.[4,5,6,7] However, ZMA suffers from its spontaneous reaction with protons and water molecules in the aqueous electrolytes—hydrogen evolution reaction (HER)[8]—which causes irreversible zinc corrosion. HER results in a low CE, shortened battery longevity, a higher LEC, and potentially a safety hazard. In addition, the non-flat surface morphology of ZMA, often dubbed as dendrites, is common for plated Zn during battery charging,[9,10] which increases ZMA's reactive surface area, thus further promoting the HER reaction and sometimes causing the electrolyte to be dried out.[11] The Zn dendrites may short-circuit the battery, leading to a catastrophic battery failure. In addition, HER increases the local pH values near the electrode surface, causing precipitation of byproducts such as $Zn(OH)_2$ and $ZnSO_4[Zn(OH)_2]_3 \cdot xH_2O$,[12] which in turn also degrades the CE and overall battery performance.[13]

Progress has been made to inhibit HER off the surface of ZMA, including lowering water's activity by using highly concentrated electrolytes such as "Water-in-Salt" electrolytes (WiSE) and deep eutectic solvents (DES),[14] engineering the solvation structures of the aqueous solutions to promote the O–H bond strength, and growing a protective solid electrolyte interphase (SEI) layer on the surface of ZMA. The SEI formation over the graphite anode was partially responsible for the initial commercialization of Li-ion batteries in early 1990s.[15] An effective SEI passivates the surface of electrodes and nearly shuts down the parasitic reactions during the life span of the battery operation.[16,17] Unfortunately, unlike non-aqueous electrolytes for Li-ion batteries, the solvent of aqueous electrolytes—water—cannot contribute to the SEI formation because its electrolytic products, either the gaseous products or the generated protons and hydroxide ions, are unlikely to be constituents of the protective phase. Therefore, aqueous electrolytes require an tailor-designed SEI to be formed with the assistance of electrolyte additives or co-solvent.[18] To date, some organic additives in the electrolytes have been demonstrated effective in creating protective layers on the ZMA surface,[19,20] including silk fibroin proteins,[21] sodium dodecyl sulfate,[22] and dimethyl carbonate,[23] where the electrolytes investigated are often dilute ones. Among the additives, vanillin is a promising candidate as it is nontoxic, abundant, and widely employed as a corrosion inhibitor for different metals such as copper,[24] aluminum,[25] and stainless steel.[26] Vanillin has been investigated in 2 M $ZnSO_4$ as an additive, which increases the CE of ZMA to 99.8%, tested at 1 mA/cm^2.[27] However, this electrolyte formula exhibits a CE of 97.56% at 0.2 mA/cm^2, as we revealed (**Figure S1**). Note that a lower current density can better reveal the impacts of HER, and the CE of ZMA is usually lower when evaluated at a low current density due to the less-masked impacts of HER. To date, there have been few studies of growing SEI on ZMA in highly concentrated electrolytes, even though such electrolytes are effective in suppressing dendrite formation on ZMA and generally improving the CE by minimizing water's activity in the electrolytes.

The dendrite formation relates to the formation of an ion-depletion layer formed near the electrode surface during the plating process.[28] A high concentration of both anions and cations may suppress the dendrite formation to some extent because the ions are too crowded to be completely depleted, where, to this end, WiSE have been demonstrated helpful.[29,30,31] In WiSE, the interactions between cations and anions intensify to generate ion pairs, where the Zn plating

can bring fluorinated anions to be reduced on the electrode surface, thus paving a fluoride-rich SEI layer. Nevertheless, fluorinated WiSE are challenged by their high cost and potentially detrimental environmental impacts. Among alternative WiSE, concentrated $ZnCl_2$ electrolytes have engendered much interest due to its low cost and high solubility of $ZnCl_2$ up to 31 *m* (molality or moles/kg of solvent) at room temperature. Unfortunately, a WiSE of 30 *m* $ZnCl_2$ can only deliver an average CE of 95.38% for ZMA at 0.2 mA/cm^2 and the plated Zn surface still features a rough platelet morphology (**Figure 2A**). The pure $ZnCl_2$ electrolyte does not appear to create an effective SEI. Furthermore, the concentrated $ZnCl_2$ exhibits a unique chemical environment with a high acidity that may explain the relatively low CE. In this study, we investigated the impacts of vanillin as an electrolyte additive for 30 *m* $ZnCl_2$. With a tiny concentration (5 mg per mL of water) of vanillin added, we observed markedly enhanced CE of ZMA up to 99.34% at 0.2 mA/cm^2, which is much higher than the dilute counterparts with vanillin added.[27] Our characterization suggests that vanillin is chlorinated in the acidic 30 *m* $ZnCl_2$ electrolyte, where the resulting less-soluble product precipitates on the ZMA's surface as an effective SEI layer. The SEI formation mechanism here differs from the known protection mechanisms based on cathodic decomposition of additives.[32]

2. Results and Discussion:

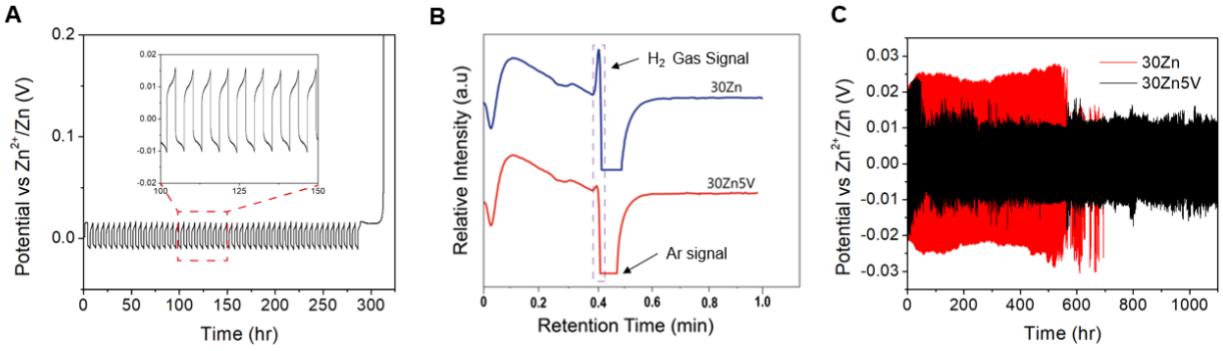

Figure 1. Electrochemical studies on the stability of the electrolytes. A) GCD potential profiles to test an average CE via an asymmetric Zn||Zn cell at 0.2 mA/cm^2, where the working Zn electrode is a Zn foil that is 10 µm thick and the counter electrode has an excess of Zn by being 100 µm thick. B) Gas chromatography (GC) results of 30Zn (blue) and 30Zn5V (red) in argon gas. C) Cycling stability tests of Zn metal anodes with the two different electrolytes at 1 mA/cm^2.

We measured the CE of electrolytes based on 30 *m* $ZnCl_2$ with varying concentrations of vanillin as an additive, *i.e.*, 0, 2, 5, and 8 mg/mL$_{water}$, which are denoted as 30Zn, 30Zn2V, 30Zn5V, and 30Zn8V, respectively. CE was calculated with the following equation:

$$CE = \left(1 - \frac{Q_t - Q_s}{nQ_c}\right) * 100\% \quad (1)$$

where n is the number of cycles, Q_c corresponds to a fixed percentage (10%) of the total capacity (Q_t) of the Zn foil that is 10 µm thick, and lastly Q_s is the capacity from the final stripping process after n cycles, where the ZMA is biased to an upper cutoff potential of 0.2 V. We

measured the purity of the Zn foil of the working electrode by a complete stripping, which is on average 96.8%, and this value is factored in to calculate Q_t. This equation is a more accurate representation of the CE when using our testing methodology with an existing ZMA working electrode.[33,34] The CE of each electrolyte was calculated by averaging over five runs, yielding CE values of 95.38%, 98.30%, 99.34%, and 98.60% for 30Zn, 30Zn2V, 30Zn5V, and 30Zn8V, respectively (**Figure S2**). The overall trend suggests the utility of vanillin in improving the CE values.

To gain insights on why vanillin increases the CE of ZMA, we focus our attention on 30Zn5V in comparison with 30Zn. To quantify the extent of HER, a Zn||Zn symmetric beaker cell was run at a current density of 1 mA/cm^2 for 3 hours, which yielded a total amount of 0.805 mmol of H_2 in the 30Zn electrolyte, but only 0.103 mmol of H_2 in 30Zn5V (**Figure 1B**). Thus, HER is suppressed during cycling with the presence of vanillin.

The plating/stripping stability of ZMA is greatly improved in the presence of vanillin in the electrolyte. Our tests cycled symmetric Zn||Zn cells with different electrolytes at 1 mA/cm^2 until a failure occurred. The 30Zn electrolyte could run for 550 hours with an overpotential of ca. 0.025 V before experiencing unstable behaviors and ultimately failed around the 650-hour mark (**Figure 1C**). On the other hand, the 30Zn5V electrolyte started out with a similar overpotential as 30Zn does, but after 50 cycles, the overpotential decreased to 0.015 V and stayed relatively consistent for 1100 hours before a power outage halted the experiment prematurely. The overpotential drop during the initial cycling in 30Zn5V is reproducible (**Figure S3)**, which suggests that there may be a conditioning process on the ZMA's surface during initial cycling, which renders the Zn plating more conducive. The minor fluctuations in the potential profile of 30Zn5V can be attributed to the varying thickness of the SEI layer on the zinc electrode. Overall, the stable cycling in 30Zn5V corroborates with the high CE.

Next, we evaluated the surface morphology of ZMA after cycling. In order to retain the plated morphology, we used symmetric Zn||Zn beaker cells to cycle the ZMA for 100 cycles at 1 mA/cm^2, where the plated Zn is allowed to grow pressure free. SEM imaging shows that the presence of vanillin in the electrolyte transforms the plated surface morphology of the ZMA from a platelet one (**Figure 2A**) to a fairly smooth surface (**Figure 2B**), similar to that of the pristine Zn foil (**Figure S4**).

With the desire to further understand why the morphology was so different even though the conditions that the cells were cycled under were nearly the same, except for the presence of vanillin, we performed energy dispersive X-ray spectroscopy (EDX) measurements to analyze the elemental makeup of the ZMA surface cycled in 30Zn and 30Zn5V (**Figure S4**). The results showed an elevated concentration of carbon on the electrode cycled in 30Zn5V, which can only come from the decomposed or adsorbed vanillin (**Figure 2C**). In addition, the average contact angles of the electrode surface to water are 84° after cycling for 100 cycles in 30Zn and 102° in 30Zn5V, where one explanation is that vanillin or its derivative covers the surface of ZMA, turning it more hydrophobic (**Figure S5**).

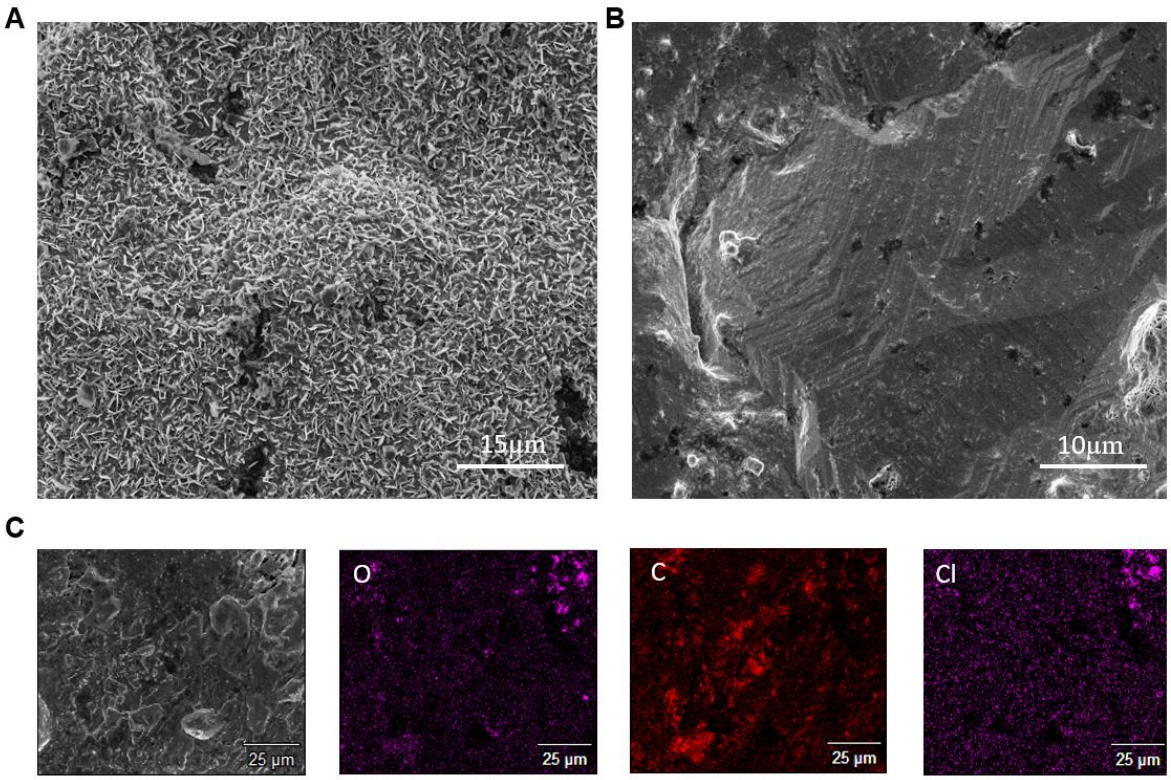

Figure 2. Microscopy results of the ZMA surfaces after cycling for 100 cycles at 1 mA/cm^2. A and B) SEM images after cycling in 30Zn and 30Zn5V, respectively. C) EDX elemental mapping after cycling in 30Zn5V.

The mechanism by which vanillin enhances CE could either be through manipulating the bulk electrolyte, or something that it does on the ZMA surface. In previous studies, it was reported the vanillin can be physically adsorbed on the ZMA's surface to form a protective layer.[27] We recently reported that dimethyl carbonate (DMC) gets reduced by Zn metal surface, thus contributing to the formation of an SEI layer.[18] Here, we examine whether vanillin's adopts a similar mechanism. We first conducted linear sweep voltammetry (LSV) to measure the potentials for plating Zn from 30Zn and 30Zn5V, obtaining values of –0.730 V and –0.743 V respectively (**Figure 3A**). Remarkably, as revealed by the inset, the two electrolytes exhibit nearly the same reduction behavior, which negates the postulation of vanillin's cathodic decomposition at the Zn metal surface. On the other hand, the LSV results support the notion that there exists an SEI layer on ZMA as a lower potential is needed to plate Zn from 30Zn5V as an SEI layer can cause Ohmic resistance and lower the activity of Zn^{2+} near the ZMA's surface. We further evaluated the redox potentials of the Zn metal anode in 30Zn and 30Zn5V by the Tafel plots, which are –0.708 V and –0.717 V, respectively, confirming the LSV results (**Figure 3B**). In addition, the exchange current densities for 30Zn and 30Zn5V are 1.40 mA/cm^2 and 0.32

mA/cm^2, respectively. The lower exchange current densities in 30Zn5V further suggests that the ZMA surface is furnished by an SEI layer.

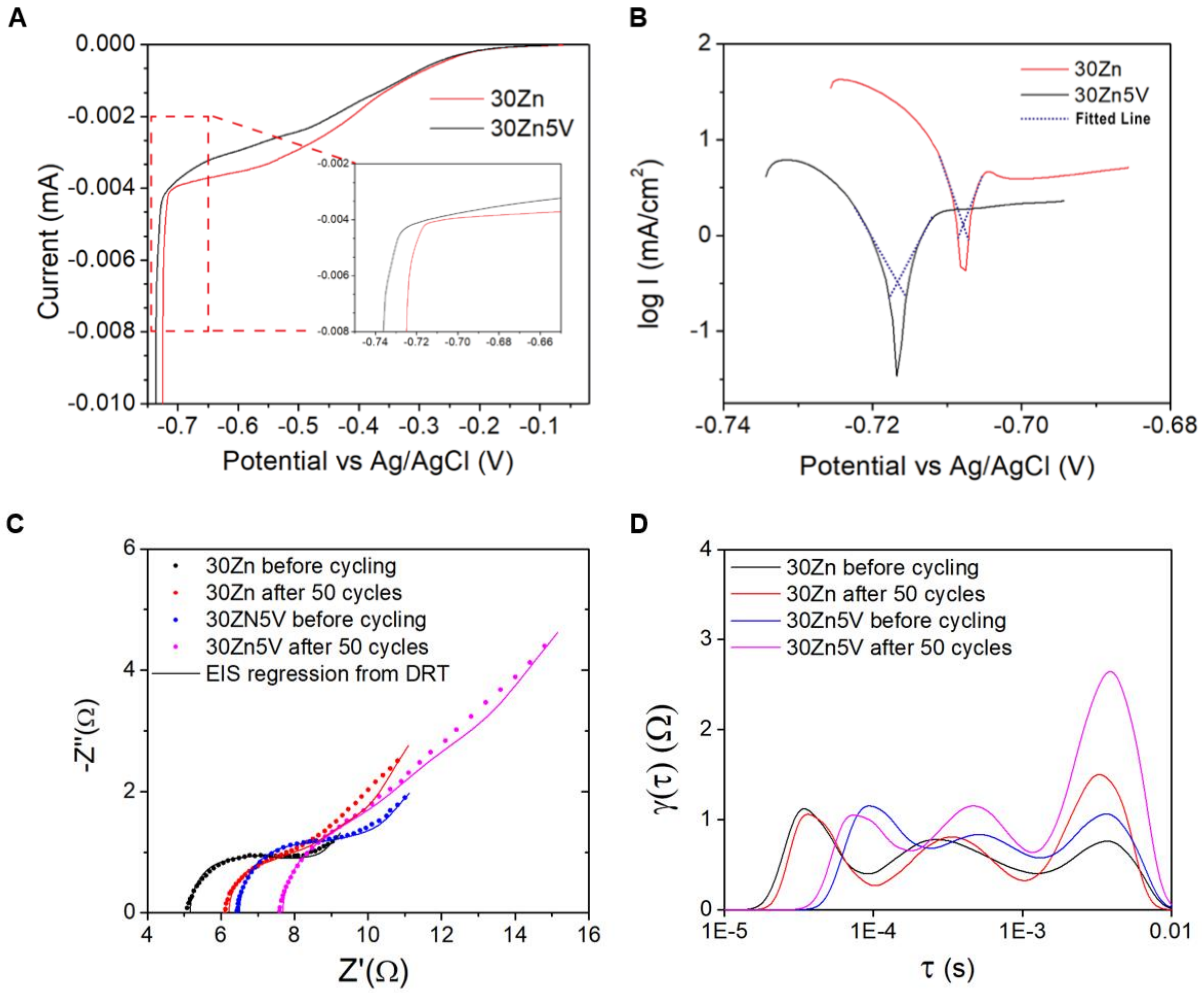

Figure 3. A) Cathodic LSV profiles at 0.1 mV/s collected in three-electrode Swagelok® cells with Ag/AgCl as the reference electrode, Ti rod as the working electrode, and Zn foil as the counter electrode. B) Tafel plots of Zn anodes in electrolytes with and without vanillin. C) Nyquist plots before and after 50 cycles collected in a Zn||Zn symmetric cell using both 30Zn and 30Zn5V, cycled at a current density of 1 mA cm^{-2} and a capacity cut-off of 1 mAh cm^{-2}. D) Distribution of Relaxation Times (DRT) calculated from EIS data. Nyquist plots generated from the DRT results are plotted on C) to validate the fitting.

To further delve into the SEI development of the cycling process, we ran electrochemical impedance spectroscopy (EIS) measurements of Zn||Zn symmetric cells with 30Zn and 30Zn5V electrolytes before and after 50 cycles of plating and stripping. While both cells show enlarged impedance after cycling, 30Zn5V shows a more significant increase (**Figure 3C**). Note that the increase in the equivalent series resistance is mainly due to the electrolyte evaporation as the

Swagelok® cells are not completely hermetic. However, it is challenging to quantify the influence of the SEI formation by examining the Nyquist plot alone. To determine the contribution due to the SEI growth to the impedance increase, we conducted a distribution of relaxation times (DRT) analysis to deconvolute the impedance data into several RC parallel circuits with different time constants (**Figure 3D**). The fitting Nyquist plots calculated from the DRT results (solid lines) are plotted over the experimental data (dotted lines) in Figure 3C to validate the DRT results. All EIS spectra collected show three peaks in DRT results, which can be ascribed to three physical interfaces of the Zinc electrode. The peak with the lowest time constant can be assigned as the Ti|Zn interface, where the electronic contacts do not change throughout the cycling.[35] The next peak should be attributed to the charge transfer across the Zn|SEI interface, as it is evident that electron transfer on the Zn metal surface is faster than ion migration through the SEI layer. Lastly, the peak with the longest time constant that shows the largest increase in the resistance after cycling is assigned to the ion transport through the SEI. Therefore, it is evident that the cycling in 30Zn5V gives rise to forming an SEI layer, doubling the interphase resistance increase compared to 30Zn.

To this point, a critical question is whether vanillin is physically adsorbed on the surface of ZMA or it is decomposed there. To probe the nature of the ZMA's surface coating, we collected X-ray photoelectron spectra (XPS), where the carbon peak can be deconvoluted into four peaks at 284.3 eV, 286.1 eV, 288.0 eV, and 289.7 eV, which correspond to C–H bonds, C–O single bond, C–Cl bond, and C=O double bond, respectively (**Figure 4A**). The XPS results for chloride yield two peaks after fitting, where the first at 200.5 eV belongs to organic chloride bonds, *i.e.,* C–Cl, while the peak at 198.4 eV is attributed to Zn–Cl bonds (**Figure 4B**). The chloride peaks indicate that vanillin decomposes to constitute to the surface coating.

What causes the decomposition of vanillin, and does it happen in the bulk electrolyte or on ZMA surface during cycling? To answer these, we characterized the electrolytes by conducting liquid-state ^{13}C NMR and ^{1}HNMR to find out whether there are detectable byproducts of the vanillin decomposition reaction. We dissolved vanillin 5 ppm in D_2O to collect a background spectrum of ^{13}C NMR of vanillin. Two other electrolyte conditions were tested: 30 *m* $ZnCl_2$ with vanillin solvated and rested for 60 days at room temperature, and the 30Zn5V electrolyte collected after 100 cycles of plating-stripping processes in a symmetric Zn||Zn cell. The spectrum of vanillin solvated in pure D_2O exhibits a very prominent peak at 195 ppm that corresponds to the carbon in the aldehyde of vanillin. However, the intensity this peak diminishes after vanillin is solvated in 30 *m* $ZnCl_2$ for 60 days (**Figure 4C**). Furthermore, the aldehyde peak vanished after 100 cycles; nevertheless, a new peak at 18 ppm emerged from the cycling process, which is indicative of a sp^3 hybridized carbon. In the ^{1}H NMR, we observed an intensity decrease of the aldehyde proton (**Figure S6**), which is consistent with the notion that the aldehyde hydrogen becomes hydrogen on a sp^3 carbon, thus comporting with the XPS results.

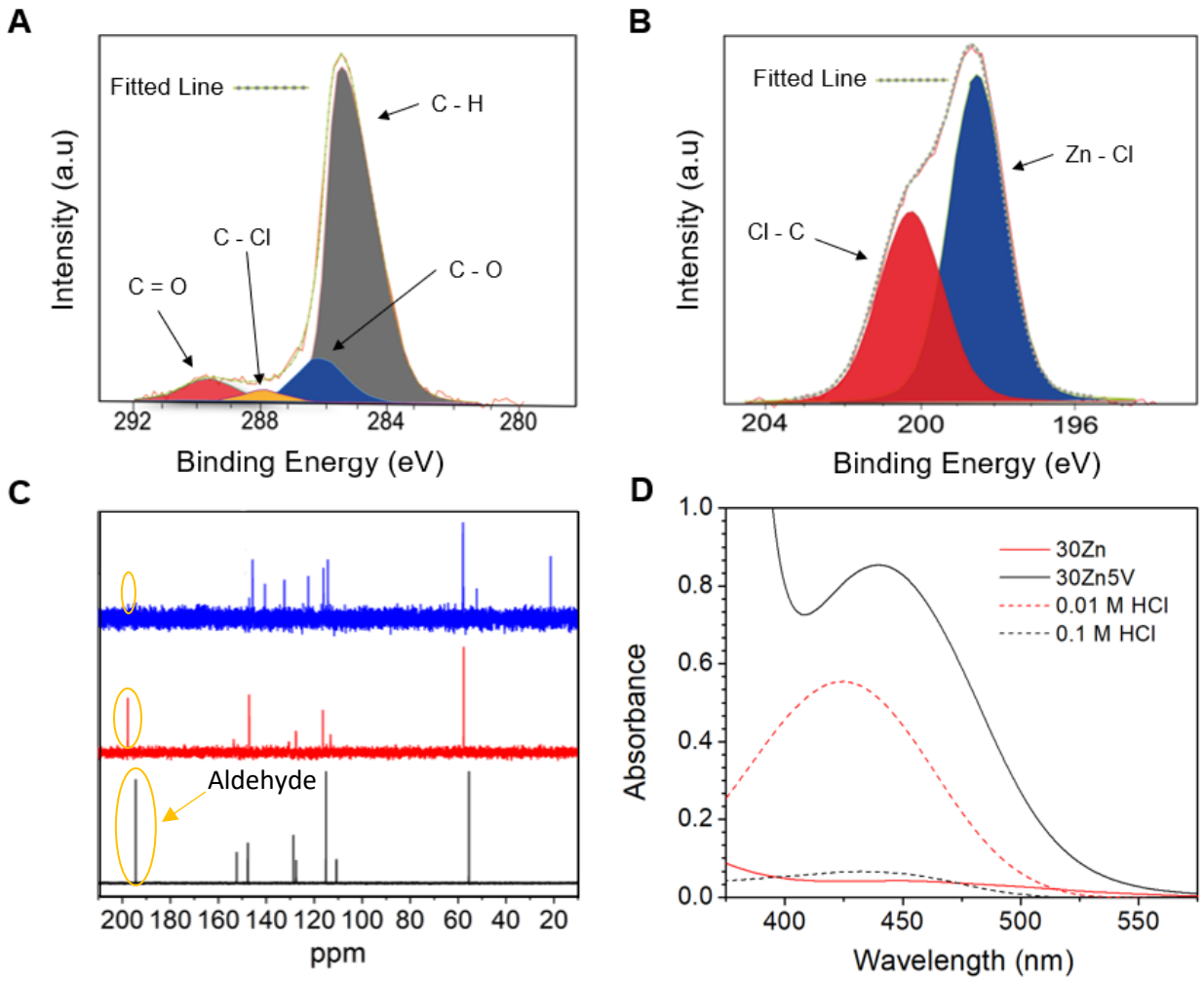

Figure 4. A and B) XPS spectra of carbon and chlorine off the surface of cycled ZMA. C) ^{13}C-NMR spectra taken for a solution with vanillin dissolved in D_2O (black), resting 60 days with vanillin solvated in 30 *m* $ZnCl_2$ (red), and 30Zn5V electrolyte (blue) after 100 cycles of plating-stripping in a symmetric Zn||Zn cell. D) UV-Vis spectra used to calculate the Hammett acidity.

With all the data we have acquired, we postulate that protons attack the aldehyde carbon of vanillin in the acidic environment of 30 *m* $ZnCl_2$, creating an intermediate, **2**. Later, Cl^- neutralizes **2** by attacking its carbon and turning it into a sp^3 carbon, forming an even less soluble compound, **3**, thus being precipitated to form an SEI layer **(see Figure 5A)**. If vanillin's reaction requires protons, the addition of vanillin in 30 *m* $ZnCl_2$ may alter the acidity of this electrolyte. We tested the Hammett acidity of 30 *m* $ZnCl_2$ before and after adding vanillin, finding that vanillin dramatically decreases the electrolyte acidity from –2.08 in 30 *m* $ZnCl_2$ to –0.23 in 30Zn5V (**Figure 4D** and **Figure S7**).[36,37]

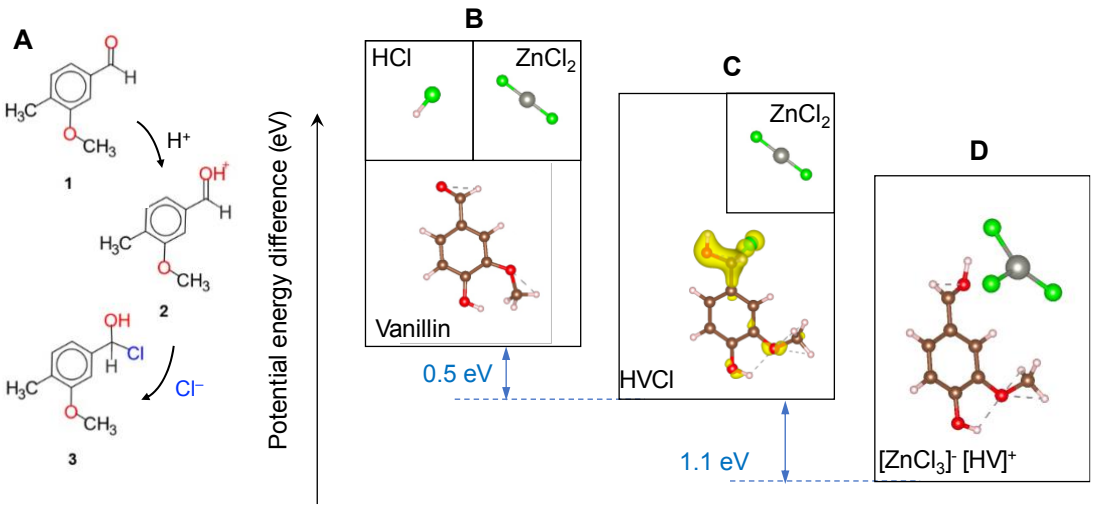

Figure 5. A) Proposed mechanism for the decomposition of vanillin in 30 *m* $ZnCl_2$. B-D) DFT computed energy differences between vanillin, HVCl, and the protonated $[HV]^+$ cation in the presence of Zn-Cl species.

Two sets of density functional theory (DFT) calculations were performed to help interpret the characterization results and elucidate the mechanism of SEI formation. The first set of calculations examined whether the vanillin-based mechanism identified in dilute $ZnCl_2$ electrolytes[27] could also be responsible for the improved CE we observed in highly concentrated electrolytes, where Zn^{2+} ions outnumber vanillin by ca. 900:1. In this study we examined the energetics of vanillin displacing H_2O from the first solvation shell of $[ZnCl]^+$ at a ZMA surface (**Figure S8**). We found that, while there is a strong potential energy incentive for vanillin to displace one water molecule from the first solvation shell of Zn^{2+}, steric effects from the large vanillin molecules mean that the energy gain from replacing the remaining water is comparable with thermal energy and thus negligible. It is clear that in these concentrated electrolytes vanillin's mechanism for suppressing the HER is different from that identified in dilute electrolytes. Thus, in a second DFT study we examined the energetics of the proposed vanillin decomposition by electrophilic addition, followed by chlorination of the aldehyde carbon to form a molecule with a formula ($C_8H_9O_3Cl$) shown in **Figure 5C,** which we refer to using the shorthand HVCl. In Figure 5C, we have also plotted the sum of the charge density from the wave functions containing the largest contribution from the aldehyde carbon's atomic orbitals, which shows a clear sp^3 character consistent with the XPS results for the SEI of the cycled anode. To understand how this derivative of vanillin could affect the solvation environment of Zn^{2+}, we performed calculations to probe the interaction of HVCl with various $[ZnCl_3]^-(H_2O)_n$ and $ZnCl_2{\cdot}(H_2O)_n$ solvation structures. In each case, the HVCl molecule spontaneously decomposed during relaxation, leaving the protonated vanillin cation (HV^+). One example with n=0 is shown in **Figure 5D**. This implies that HVCl is not stable in the bulk electrolyte and explains why a reduction in the 195 ppm ^{13}C-NMR peak is observed in 30Zn5V, but no covalently bonded Cl is observed in XPS spectra of the electrolyte until it is cycled in the presence of ZMA. This leads us to propose that protonated vanillin cations that form spontaneously in the highly acidic electrolyte act as an irreducible co-salt that can take up the

excess Cl^- ions that are given up when $[ZnCl]^+$ ions are reduced. As HVCl also binds more strongly to the ZMA surface than vanillin (**Figure S9**), these molecules create a passivating layer that inhibits HER.

While the DFT results are consistent with the spectroscopic results, strongly indicating the presence of HVCl in the SEI, it is not clear if the ability of HV^+ to covalently bond to Cl^- to form HVCl is necessary for the functionality of the SEI. In other words, when searching for other electrolyte additives, it remains to be known if it is sufficient for an additive to form a protonated cation and have favorable binding to ZMA, or if the covalent interaction with Cl^- also required.

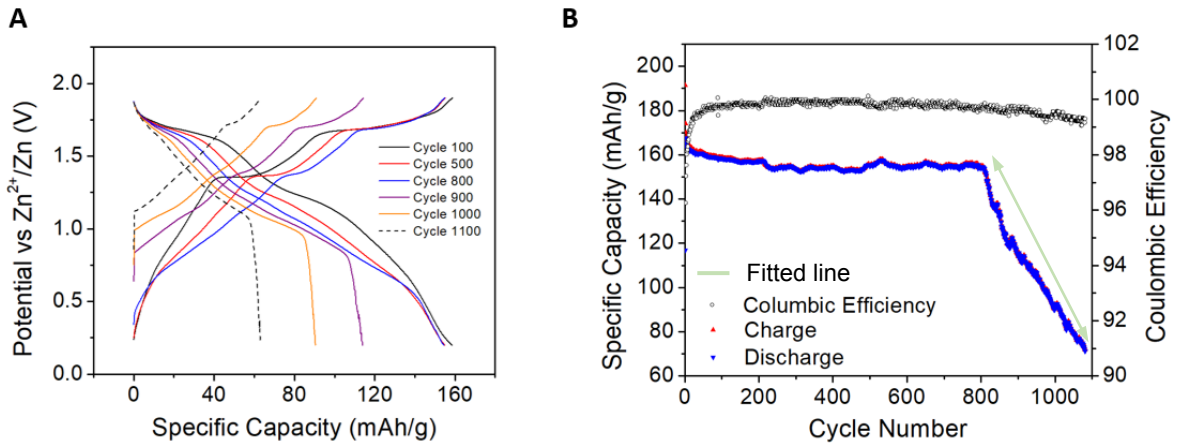

Figure 6. Electrochemical performance of $VOPO_4 \cdot 2H_2O$||Zn full cells. A) GCD potential profiles at 100 mA/g with an N:P ratio of 2:1 of different cycles. B) The cycling in a Swagelok® cell with an active mass loading of 16 mg/cm^2 of the cathode at a current rate of at 100 mA/g.

To test the practicality of this electrolyte, multiple $VOPO_4$||Zn full cells were made with an N/P ratio of 2:1, which were cycled at a current rate of 100 mA/g (**Figure 6A**). One representative cell was able to run for 818 cycles without fading, delivering an average specific capacity of 156 mAh/g (based on the cathode). After 818 cycles, the cell capacity fades steadily. Note that our previous studies showed that the capacity of $VOPO_4$ in $ZnCl_2$-based electrolytes does not fade over thousands of cycles.[18] Therefore, the cell's capacity fading here can only be explained by the insufficient active mass of ZMA. This consideration is supported by the GCD profiles of the $VOPO_4$ cathode for the 900th, 1000th, and 1100th cycles, where the upper plateau in the GCD profiles is shortened along with the progress of cycling by providing its capacity contribution of 23 mAh/g, 12 mAh/g, and 2 mAh/g, respectively, indicating that a "full" charging cannot be completed due to the limited supply of Zn mass from ZMA. Based on the N/P ratio, it can be suggested that the initial 818 cycles consumed ca. 50% of all ZMA, based on which, an average CE of 99.92% can be estimated for the ca. 800 cycles. Note that the current rate of 100 mA/g based on the cathode mass can be translated to a current density of 1.6 mA/cm^2 for both electrodes (**Figure 6B**). The much higher CE revealed here is ascribed to the higher current density applied on the ZMA and the masked HER, aforementioned. After 818 cycles, the capacity fades at an average rate of 1.5 mAh/g, where the fading rate corresponds to an average

CE of 99.63% in each cycle. The results here suggest ZMA reacts with the electrolyte at a progressively increasing rate, which can be attributed to the wasted inactive Zn mass produced over cycling. This is the first example of using a full cell's capacity fading rate to estimate the practical CE of zinc metal anode.

3. Conclusions:

We have revealed that the acidic nature of 30 *m* $ZnCl_2$ decomposes vanillin to form a unique SEI on ZMA's surface that aids in more reversible cycling of ZMA. Through characterization, we elucidated a new mechanism for the SEI formation with vanillin, in which proton and chloride sequentially attack vanillin and cause it to be precipitated on ZMA's surface. This differs from the conventional wisdom that SEI grows via cathodic reactions with the anode's surface. The CE of the cell increases from 95.38% to 99.34% tested at a current density of 0.2 mA/cm^2, with the addition of a small amount of vanillin at the ppm scale into 30 *m* $ZnCl_2$. Furthermore, with an N/P ratio of 2:1, ZMA supports the $VOPO_4$||Zn full cell's cycling for 818 cycles before half of it is consumed, demonstrating a CE of 99.92% at a current density of 1.6 mA/cm^2. With the results of this paper, we show how a non-toxic, organic additive, *i.e.,* vanillin, can transform the performance of 30 *m* $ZnCl_2$ as an electrolyte for ZMA. Therefore, the results showcase the importance of SEI formation as a resolution to enable ZMA to be completely reversible, ultimately leading to the development of viable aqueous zinc metal batteries in the future.

4. Experimental Section

Material Preparation: The zinc foil with different thicknesses (10 μm and 100 μm) was purchased from Thermo Scientific™ and Alibaba, respectively. The vanadyl (V) phosphate dihydrate ($VOPO_4 \cdot 2H_2O$) powder was synthesized following the method described in our prior studies. [38] The chemicals of vanadium (V) oxide (>97.0%) (V_2O_5) and phosphoric acid (ACS reagent, ≥85 wt.% in H_2O) (H_3PO_4) were both purchased from Sigma Aldrich. In the synthesis of $VOPO_4$, 4.8 g of V_2O_5 was suspended in 26.6 mL of H_3PO_4 (85%) and 115.4 mL of DI water. The suspension was stirred for one hour at room temperature and then refluxed at 110°C for 16 hours. The yellow-green suspension was centrifuged, washed with DI water, and kept under vacuum. For the electrolyte preparation, the zinc chloride (metal basis, 99.95%) and water (HPLC grade) were purchased from Alfa Aesar. Vanillin (99%) was purchased from Sigma Aldrich.

Materials Characterization: SEM and EDX studies were conducted on an FEI Quanta 600F Environmental SEM. Contact-angle measurements were done on FTA125. XPS studies were carried out using a PHI VersaProbe III Scanning XPS Microprobe. ^{13}C NMR studies were performed on a Bruker Ascend 500 NMR spectrometer at a frequency of 500 MHz. Hammett acidity studies were performed on a UV-vis spectrum Lambda 1050 with an integrated sphere. HER measurements were completed on a PerkinElmer Clarus 480 gas chromatography (GC). The GC was equipped with a 5 Å molecular sieve column with Ar as the carrier gas and a thermal conductivity detector.

Electrochemical measurements: The $VOPO_4 \cdot 2H_2O$ cathode was made of 50 wt.% $VOPO_4 \cdot 2H_2O$, 40 wt.% KetjenBlack, and 10 wt.% polytetrafluoroethylene (PTFE) binder. The free-standing film electrodes were punched out to fit a Swagelok® cell and measured with an area of 0.785

cm^2. Symmetric Zn||Zn beaker cells were used to characterize the SEI with XPS, EDX, SEM, contact angle measurements, and GC. The zinc electrodes would be rinsed with DI water three times before being placed inside a vacuum chamber. The LSV and Tafel plots were measured on a VMP-3 multichannel workstation with Ti||Ti and Zn||Zn Swagelok® cells, respectively. The GCD cycling data were collected on a Landt CT3002AU. For EIS measurements, we used the same setup for the Tafel plot measurement, and the AC signal with the amplitude of 10 mV was used to scan a frequency range from 200 kHz to 10 Hz, 10 points for one decade and evenly spaced in the logarithm scale. The DRT analysis of the EIS data was conducted using DRTtools.[39] The default parameters were used throughout the analysis.

5. Computational Methods

All DFT calculations were performed using the Vienna *Ab initio* Simulation Package (VASP).[40] This computational approach employs projector augmented wave (PAW) potentials,[41] and the exchange-correlation function adopts the generalized gradient approximation (GGA) as proposed by Perdew-Burke-Ernzerhof.[42] The energy cutoff was set to be 520 eV and the Bloch vectors (*i.e.*, k-points) for sampling the Brillouin zone were set to 1x1x1. For the dispersion energy correction, we applied the DFT-D3 method with the Becke-Johnson damping function,[43] which is geometry dependent. During the geometry relaxation, we utilized the positions and stress tensor so that the cell shape (and volume) remains constant. In addition, we adopted the implicit solvent model[44] in the calculation of potential energy differences between vanillin, HVCl, and the protonated $[HV]^+$ cation in the presence of $ZnCl_2$. For the calculations involving the Zn substrate (6x6x3 unit cell), we also applied the constraints to the bottom layer atoms so that during the ionic relaxation, only surface atoms are relaxed.

Supporting information

Supporting Information is available from the Wiley Online Library

Acknowledgements

X.J. and P.A.G. thank the financial support from the U.S. NSF Award CBET-2038381 (X.J.) and CBET-2038366 (P.A.G.). This work made use of instruments in the Electron Microscopy Service and Nuclear Magnetic Resonance Facility (OSU).

Conflict of Interests

The authors declare no conflict of interests.

References

[1] Ji, X. A Perspective of $ZnCl_2$ Electrolytes: The Physical and Electrochemical Properties. *eScience* **2021**, *1* (2), 99–107.

[2] Zhang, C.; Shin, W.; Zhu, L.; Chen, C.; Neuefeind, J. C.; Xu, Y.; Allec, S. I.; Liu, C.; Wei, Z.; Daniyar, A.; Jiang, J. X.; Fang, C.; Alex Greaney, P.; Ji, X. The Electrolyte Comprising More Robust Water and Superhalides Transforms Zn-Metal Anode Reversibly and Dendrite-Free. *Carbon Energy* **2020**, *3* (2), 339–348.

[3] Dunn, B.; Kamath, H.; Tarascon, J.-M. Electrical Energy Storage for the Grid: A Battery of Choices. *Science* **2011**, *334* (6058), 928–935.
[4] Suo, L.; Borodin, O.; Gao, T.; Olguin, M.; Ho, J.; Fan, X.; Luo, C.; Wang, C.; Xu, K. "Water-in-Salt" Electrolyte Enables High-Voltage Aqueous Lithium-Ion Chemistries. *Science* **2015**, *350* (6263), 938–943..
[5] Xie, J.; Liang, Z.; Lu, Y.-C. Molecular Crowding Electrolytes for High-Voltage Aqueous Batteries. *Nature Materials* **2020**, *19* (9), 1006–1011.
[6] Wan, F.; Zhang, L.; Dai, X.; Wang, X.; Niu, Z.; Chen, J. Aqueous Rechargeable Zinc/Sodium Vanadate Batteries with Enhanced Performance from Simultaneous Insertion of Dual Carriers. *Nature Communications* **2018**, *9* (1).
[7] Zhao, Z.; Zhao, J.; Hu, Z.; Li, J.; Li, J.; Zhang, Y.; Wang, C.; Cui, G. Long-Life and Deeply Rechargeable Aqueous Zn Anodes Enabled by a Multifunctional Brightener-Inspired Interphase. *Energy & Environmental Science* **2019**, *12* (6), 1938–1949.
[8] Li, C.; Jin, S.; Archer, L. A.; Nazar, L. F. Toward Practical Aqueous Zinc-Ion Batteries for Electrochemical Energy Storage. *Joule* **2022**, *6* (8), 1733–1738.
[9] Ma, L.; Chen, S.; Li, N.; Liu, Z.; Tang, Z.; Zapien, J. A.; Chen, S.; Fan, J.; Zhi, C. Hydrogen-Free and Dendrite-Free All-Solid-State Zn-Ion Batteries. *Advanced Materials* **2020**, *32* (14), 1908121.
[10] Bayaguud, A.; Fu, Y.; Zhu, C. Interfacial Parasitic Reactions of Zinc Anodes in Zinc Ion Batteries: Underestimated Corrosion and Hydrogen Evolution Reactions and Their Suppression Strategies. *Journal of Energy Chemistry* **2022**, *64*, 246–262.
[11] Zeng, Y.; Zhang, X.; Qin, R.; Liu, X.; Fang, P.; Zheng, D.; Tong, Y.; Lu, X. Dendrite-Free Zinc Deposition Induced by Multifunctional CNT Frameworks for Stable Flexible Zn-Ion Batteries. *Advanced Materials* **2019**, *31* (36), 1903675.
[12] Wang, N.; Wan, H.; Duan, J.; Wang, X.; Tao, L.; Zhang, J.; Wang, H. A review of zinc-based battery from alkaline to acid. *Materials Today Advances* **2021**, *11*, 100149.
[13] Liu, C.; Xie, X.; Lu, B.; Zhou, J.; Liang, S. Electrolyte Strategies toward Better Zinc-Ion Batteries. *ACS Energy Letters* **2021**, *6* (3), 1015–1033.
[14] Li, M.; Wang, X.; Hu, J.; Zhu, J.; Niu, C.; Zhang, H.; Li, C.; Wu, B.; Han, C.; Mai, L. Comprehensive H_2O molecules regulation via deep eutectic solvents for ultra-stable zinc metal anode. *Angewandte Chemie International Edition* **2023**, *62* (8).
[15] Peled, E.; Menkin, S. Review—Sei: Past, Present and Future. *Journal of The Electrochemical Society* **2017**, *164* (7).
[16] Cao, L.; Li, D.; Pollard, T.; Deng, T.; Zhang, B.; Yang, C.; Chen, L.; Vatamanu, J.; Hu, E.; Hourwitz, M. J.; Ma, L.; Ding, M.; Li, Q.; Hou, S.; Gaskell, K.; Fourkas, J. T.; Yang, X.-Q.; Xu, K.; Borodin, O.; Wang, C. Fluorinated Interphase Enables Reversible Aqueous Zinc Battery Chemistries. *Nature Nanotechnology* **2021**, *16* (8), 902–910.
[17] Huang, W.; Wang, H.; Boyle, D. T.; Li, Y.; Cui, Y. Resolving Nanoscopic and Mesoscopic Heterogeneity of Fluorinated Species in Battery Solid-Electrolyte Interphases by Cryogenic Electron Microscopy. *ACS Energy Letters* **2020**, *5* (4), 1128–1135.
[18] Jiang, H.; Tang, L.; Fu, Y.; Wang, S.; Sandstrom, S. K.; Scida, A. M.; Li, G.; Hoang, D.; Hong, J. J.; Chiu, N.-C.; et al. Chloride electrolyte enabled practical zinc metal battery with a near-unity coulombic efficiency. *Nature Sustainability* **2023**.
[19] Li, C.; Shyamsunder, A.; Hoane, A. G.; Long, D. M.; Kwok, C. Y.; Kotula, P. G.; Zavadil, K. R.; Gewirth, A. A.; Nazar, L. F. Highly Reversible Zn Anode with a Practical Areal Capacity Enabled by a Sustainable Electrolyte and Superacid Interfacial Chemistry. *Joule* **2022**, *6* (5), 1103–1120.
[20] Yang, Y.; Liu, C.; Lv, Z.; Yang, H.; Cheng, X.; Zhang, S.; Ye, M.; Zhang, Y.; Chen, L.; Zhao, J.; Li, C. C. Redistributing Zn-Ion Flux by Interlayer Ion Channels in MG-Al Layered Double Hydroxide-Based Artificial Solid Electrolyte Interface for Ultra-Stable and Dendrite-Free Zn Metal Anodes. *Energy Storage Materials* **2021**, *41*, 230–239.
[21] Xu, J.; Lv, W.; Yang, W.; Jin, Y.; Jin, Q.; Sun, B.; Zhang, Z.; Wang, T.; Zheng, L.; Shi, X.; Sun, B.; Wang, G. In Situ Construction of Protective Films on Zn Metal Anodes via Natural Protein Additives Enabling High-Performance Zinc Ion Batteries. *ACS Nano* **2022**, *16* (7), 11392–11404.
[22] Sun, K. E.; Hoang, T. K.; Doan, T. N.; Yu, Y.; Zhu, X.; Tian, Y.; Chen, P. Suppression of Dendrite Formation and Corrosion on Zinc Anode of Secondary Aqueous Batteries. *ACS Applied Materials & Interfaces* **2017**, *9* (11), 9681–9687.

[23] Dong, Y.; Miao, L.; Ma, G.; Di, S.; Wang, Y.; Wang, L.; Xu, J.; Zhang, N. Non-Concentrated Aqueous Electrolytes with Organic Solvent Additives for Stable Zinc Batteries. *Chemical Science* **2021**, *12* (16), 5843–5852.

[24] Wang, Z.; Wang, T.; Zhu, J.; Wei, L.; Shen, Y.; Li, N.; Hu, J. Synergistic Effect and Mechanism of Copper Corrosion Inhibition Using Cinnamaldehyde and Vanillin in Hcl Solution: An Experimental and Theoretical Approach. *Colloids and Surfaces A: Physicochemical and Engineering Aspects* **2019**, *563*, 246–254.

[25] Rosliza, R.; Nora'aini, A.; Wan Nik, W. B. Study on the Effect of Vanillin on the Corrosion Inhibition of Aluminum Alloy. *Journal of Applied Electrochemistry* **2010**, *40* (4), 833–840.

[26] Quraishi, M. A.; Ansari, K. R.; Chauhan, D. S.; Umoren, S. A.; Mazumder, M. A. Vanillin Modified Chitosan as a New Bio-Inspired Corrosion Inhibitor for Carbon Steel in Oil-Well Acidizing Relevant to Petroleum Industry. *Cellulose* **2020**, *27* (11), 6425–6443.

[27] Zhao, K.; Liu, F.; Fan, G.; Liu, J.; Yu, M.; Yan, Z.; Zhang, N.; Cheng, F. Stabilizing Zinc Electrodes with a Vanillin Additive in Mild Aqueous Electrolytes. *ACS Applied Materials & Interfaces* **2021**, *13* (40), 47650–47658.

[28] Li, Li, S.; Jiang, M.; Xie, Y.; Xu, H.; Jia, J.; Li, J. Developing high-performance lithium metal anode in liquid electrolytes: Challenges and progress. *Advanced Materials* **2018**, *30* (17), 1706375.

[29] Wang, F.; Borodin, O.; Gao, T.; Fan, X.; Sun, W.; Han, F.; Faraone, A.; Dura, J. A.; Xu, K.; Wang, C. Highly reversible zinc metal anode for aqueous batteries. *Nature Materials* **2018**, *17* (6), 543–549.

[30] Zhang, C.; Holoubek, J.; Wu, X.; Daniyar, A.; Zhu, L.; Chen, C.; Leonard, D. P.; Rodríguez-Pérez, I. A.; Jiang, J.-X.; Fang, C.; Ji, X. A $ZnCl_2$ Water-in-Salt Electrolyte for a Reversible Zn Metal Anode. *Chemical Communications* **2018**, *54* (100), 14097–14099.

[31] Suo, L.; Borodin, O.; Gao, T.; Olguin, M.; Ho, J.; Fan, X.; Luo, C.; Wang, C.; Xu, K. "water-in-salt" electrolyte enables high-voltage aqueous lithium-ion chemistries. *Science* **2015**, *350* (6263), 938–943.

[32] Azhagurajan, M.; Nakata, A.; Arai, H.; Ogumi, Z.; Kajita, T.; Itoh, T.; Itaya, K. Effect of Vanillin to Prevent the Dendrite Growth of Zn in Zinc-Based Secondary Batteries. *Journal of The Electrochemical Society* **2017**, *164* (12).

[33] Adams, B. D.; Zheng, J.; Ren, X.; Xu, W.; Zhang, J. Accurate Determination of Coulombic Efficiency for Lithium Metal Anodes and Lithium Metal Batteries. *Advanced Energy Materials* **2017**, *8* (7), 1702097.

[34] Mohammadi, A.; Djafer, S.; Sayegh, S.; Naylor, A. J.; Bechelany, M.; Younesi, R.; Monconduit, L.; Stievano, L. Assessing Coulombic Efficiency in Lithium Metal Anodes. *Chemistry of Materials* **2023**, *35* (6), 2381–2393.

[35] Shaw, L.; Chen, C.; Lin, H.; Liu, B. *Deconvolution of the electrochemical impedance of Na/Nacro2 cells with ester- and ether-based electrolytes* **2023**.

[36] Jolly, W. J. In *Modern Inorganic Chemistry*; McGraw-Hill, New York City, NY, USA **1985**; pp 202–203.

[37] Duffy, J. A.; Ingram, M. D. Acidic nature of metal aquo complexes: Proton-transfer equilibriums in concentrated aqueous media. *Inorganic Chemistry* **1978**, *17* (10), 2798–2802.

[38] Xu, Y.; Wu, X.; Sandstrom, S. K.; Hong, J. J.; Jiang, H.; Chen, X.; Ji, X. Fe-ion Bolted $VOPO_4 \cdot 2H_2O$ as an Aqueous Fe-ion Battery Electrode. *Advanced Materials* **2021**, *33* (49), 2105234.

[39] Wan, T. H.; Saccoccio, M.; Chen, C.; Ciucci, F. Influence of the Discretization Methods on the Distribution of Relaxation Times Deconvolution: Implementing Radial Basis Functions with DRTtools. *Electrochimica Acta* **2015**, *184*, 483–499.

[40] Fang, C.; Fan, Z. Ab Initio Molecular Dynamics Investigation of Prenucleation at Liquid–Metal/Oxide Interfaces: An Overview. *Metals* **2022**, *12* (10), 1618.

[41] Blöchl, P. E. Projector Augmented Wave Method. *Phys. Rev. B* **1994**, *50* (24), 17953–17979.

[42] Perdew, J. P.; Burke, K.; Ernzerhof, M. Generalized Gradient Approximation Made Simple. *Physical Review Letters* **1996**, *77* (18), 3865–3868.

[43] Grimme, S.; Ehrlich, S.; Goerigk, L. Effect of the Damping Function in Dispersion Corrected Density Functional Theory. *Journal of Computational Chemistry* **2011**, *32* (7), 1456–1465. DOI:10.1002/jcc.21759.

[44] Mathew, K.; Sundararaman, R.; Letchworth-Weaver, K.; Arias, T. A.; Hennig, R. G. Implicit Solvation Model for Density-Functional Study of Nanocrystal Surfaces and Reaction Pathways. *The Journal of Chemical Physics* **2014**, *140* (8).